Molecular Cell
Article

Simple Combinations of Lineage-Determining Transcription Factors Prime *cis*-Regulatory Elements Required for Macrophage and B Cell Identities

Sven Heinz,[1,7] Christopher Benner,[1,7] Nathanael Spann,[1,7] Eric Bertolino,[4] Yin C. Lin,[3] Peter Laslo,[6] Jason X. Cheng,[4] Cornelis Murre,[3] Harinder Singh,[4,5] and Christopher K. Glass[1,2,*]
[1]Department of Cellular and Molecular Medicine
[2]Department of Medicine
[3]Section of Molecular Biology
University of California, San Diego, 9500 Gilman Drive, La Jolla, CA 92093, USA
[4]Molecular Genetics and Cell Biology, The University of Chicago, 929 East 57th Street GCIS W522, Chicago, IL 60637, USA
[5]Department of Discovery Immunology, Genentech, San Francisco, CA 94080, USA
[6]Section of Experimental Hematology, University of Leeds, Leeds LS9 7TF, UK
[7]These authors contributed equally to this work
*Correspondence: ckg@ucsd.edu
DOI 10.1016/j.molcel.2010.05.004

SUMMARY

Genome-scale studies have revealed extensive, cell type-specific colocalization of transcription factors, but the mechanisms underlying this phenomenon remain poorly understood. Here, we demonstrate in macrophages and B cells that collaborative interactions of the common factor PU.1 with small sets of macrophage- or B cell lineage-determining transcription factors establish cell-specific binding sites that are associated with the majority of promoter-distal H3K4me1-marked genomic regions. PU.1 binding initiates nucleosome remodeling, followed by H3K4 monomethylation at large numbers of genomic regions associated with both broadly and specifically expressed genes. These locations serve as beacons for additional factors, exemplified by liver X receptors, which drive both cell-specific gene expression and signal-dependent responses. Together with analyses of transcription factor binding and H3K4me1 patterns in other cell types, these studies suggest that simple combinations of lineage-determining transcription factors can specify the genomic sites ultimately responsible for both cell identity and cell type-specific responses to diverse signaling inputs.

INTRODUCTION

The development of complex multicellular organisms involves hierarchically organized progenitor cells that ultimately give rise to terminally differentiated cell types with specialized functions. Cell fates are specified by lineage-determining transcription factors whose expression is often not limited to a single cell type (Tronche and Yaniv, 1992). Comparisons of the genome-wide binding patterns of different transcription factors in a variety of species and cell types have generated two major insights regarding transcription factor binding patterns: (1) different factors in the same cell type tend to colocalize on a genome-wide scale (Chen et al., 2008; MacArthur et al., 2009), and (2) the same factor in different cell types or at different stages of development exhibits different genome-wide binding patterns (Lupien et al., 2008; Odom et al., 2004; Sandmann et al., 2006).

Several mechanisms have been proposed to explain this phenomenon, including protein-protein interactions that enable ternary complex formation with DNA (Verger and Duterque-Coquillaud, 2002), pioneering factors that disrupt the closed nucleosome conformation and enable other factors to bind (Cirillo et al., 2002), cooperative binding of one or more factors to clustered sites that facilitates nucleosome displacement and stable binding of the factors involved (Boyes and Felsenfeld, 1996; Miller and Widom, 2003), and binding to chromatin marked in a cell type-specific manner by lysine 4-methylated histone H3 (H3K4me1/2) (Lupien et al., 2008), a sign of open chromatin that is correlated with activity of nearby genes (Heintzman et al., 2009). However, how transcription factors gain access to their eventual binding sites and the hierarchy of events that generate their cell type-specific binding and the associated epigenetic modification patterns have not previously been elucidated on a genome-wide scale.

The mammalian hematopoietic system represents a well-characterized model for the analysis of the combinatorial sets of transcription factors that orchestrate the development of distinct cell types from hematopoietic stem cells. Within the hematopoietic system, macrophages and B cells play essential and complementary roles in the innate and adaptive arms of the immune system. Recent studies suggest a model in which these cell types are derived from a lymphoid-primed multipotential progenitor (LMPP) that subsequently gives rise to common lymphoid progenitor (CLP) and granulocyte-macrophage progenitor (GMP) cells (Adolfsson et al., 2005) (Figure 1A). The Ets factor PU.1 is required for the generation of both GMP and

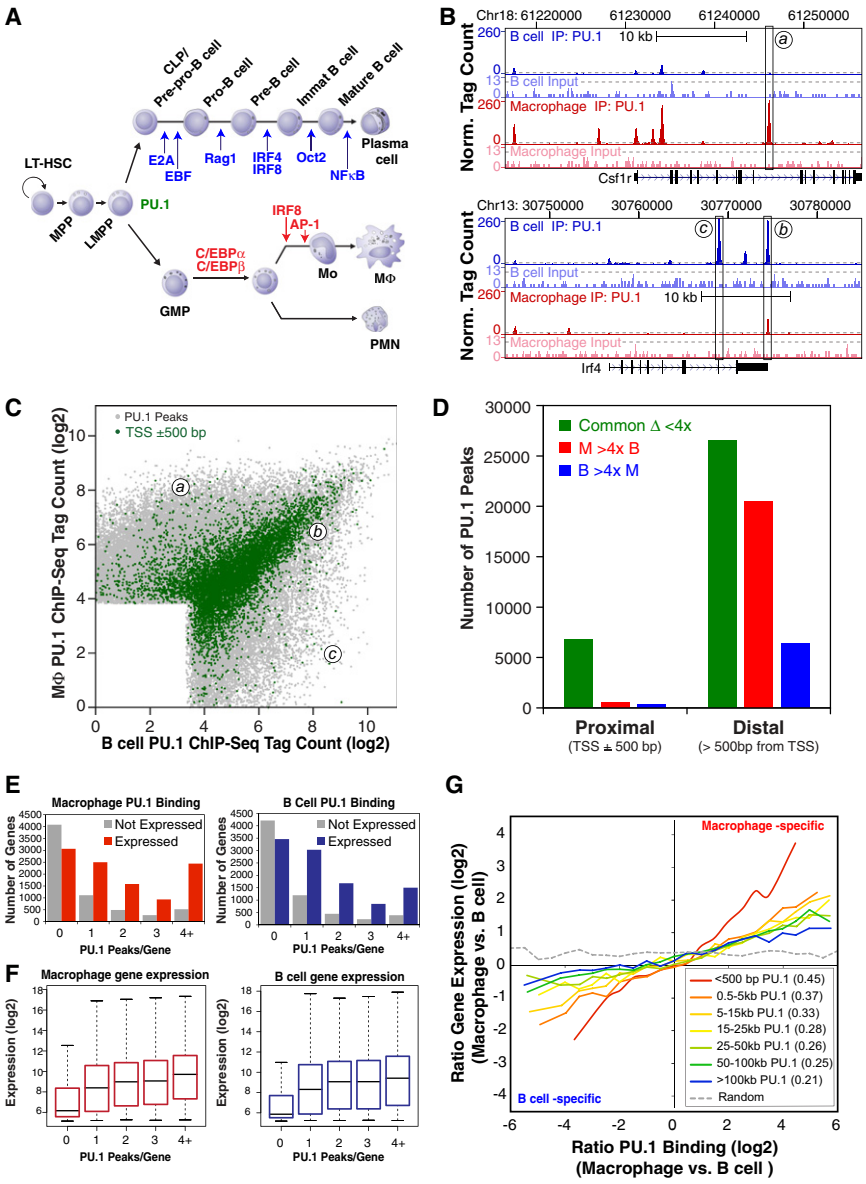

Figure 1. Identification and Functional Analysis of PU.1 Binding Sites in Primary Macrophages and Splenic B Cells

(A) Simplified scheme for macrophage and B cell differentiation from hematopoietic stem cells, indicating genetically defined factors specific for B cells (blue) and macrophages (red) at the developmental transitions most severely affected by loss of a given factor.

(B) UCSC Genome Browser image depicting PU.1 ChIP-Seq tags at the macrophage-specific *Csf1r* gene or the B cell-specific *Irf4* gene. Dashed gray lines indicate an estimated 0.1% false discovery rate (FDR). Input DNA signal is shown 10-fold magnified.

(C) PU.1-bound genomic sites are visualized by their respective normalized PU.1 ChIP-Seq tag counts (log2) within 200 bp of a given peak in macrophages and B cells. The coordinates of peaks a, b, and c from (B) are indicated. Peak positions within 500 bp of a Refseq transcription start site are colored green. Jitter was added to the normalized tag counts to visualize otherwise overlapping data points.

(D) Total number of common and cell type-specific PU.1-bound regions found in both promoter-proximal and distal genomic regions. Cell type specificity was assigned to regions with 4-fold greater normalized tag counts in one cell type relative to the other.

(E) Total number of genes with the specified number of PU.1 binding sites near their promoters. Genes were divided into subgroups of expressed and nonexpressed genes based on their absolute normalized expression levels as measured by microarray hybridization (threshold: $\log_2$(microarray signal) = 6.5).

(F) Distribution of the gene expression values for the combined subgroups of genes in the vicinity of the given number of peaks depicted in (E).

(G) Relationship between differential PU.1 binding and differential gene expression between macrophages and B cells. Subsets of PU.1 binding sites defined by their distance to the nearest TSS were sorted according to their difference in normalized tag counts between cell types. The moving average of the difference in gene expression values of the gene with the nearest TSS is reported relative to differential binding. The Pearson's correlation coefficient for each group is reported in the insert (all p values < 10^{-100}).

CLP, and the later stages of macrophage and B cell development are additionally dependent on a number of cell type-restricted factors. Of these, AP-1 and C/EBP family factors are required for macrophage development and function (Friedman, 2007), whereas E2A, EBF1, Pax5, and Oct-2 play important roles in the development and function of B cells (Medina and Singh, 2005). In addition to their roles in hematopoietic development, recent evidence suggests that PU.1-bound sites in macrophages play a role in shaping the transcriptional response to inflammatory stimuli such as lipopolysaccharide (LPS), likely by generating cell type-specific regions of open chromatin that serve as beacons for the recruitment of transcriptional coactivators in response to stimuli (Ghisletti et al., 2010).

To address the question of how lineage-determining transcription factors bind to genomic regions in a cell-specific manner, we investigated the genome-wide locations of PU.1 and the effects of loss or gain of other transcription factors on the PU.1 binding pattern in macrophages, B cells, and different B cell progenitors. In addition, we assessed the impact of loss and gain of PU.1 on the cistrome of the myeloid-restricted transcription factor, C/EBPβ. Our results suggest that cell type-specific cistromes arise from collaborative interactions between small sets of lineage-determining factors that result in enhanced DNA binding, nucleosome remodeling, and subsequent deposition of the epigenetic enhancer mark H3K4me1. The association of PU.1 and its collaborating factors at these

genomic locations provides access points for the binding of additional transcription factors, which themselves do not appear to significantly contribute to shaping the overall master regulator genomic distribution or the overall H3K4me1 pattern but act to confer transcriptional functions to these distal sites.

Distinct PU.1 Binding Programs in Macrophages and B Cells

We initially performed chromatin immunoprecipitation-coupled deep sequencing (ChIP-Seq) (Barski et al., 2007) to define the PU.1 cistromes in mouse peritoneal macrophages and splenic B cells. These analyses identified 45,631 and 32,575 PU.1-bound genomic sites (FDR < 0.1%) in macrophages and B cells, respectively (Table S1 available online), which included known PU.1 target sites (Figure S1A). Of these sites, 17,130 were independently identified as bound by PU.1 in both cell types (Figures 1B, 1C, and S1B). PU.1 was enriched at transcription start sites (TSS) relative to their genomic frequency, but the majority of binding occurred at inter- and intragenic sites (Figure S1C).

Scatter plots of the tag counts around genomic peak coordinates enable comparative visualization of experimentally observed peaks and allow the overlay of other annotations present at these genomic coordinates. (For example, the tag counts associated with PU.1 peaks at the genomic coordinates a, b, and c in Figure 1B are indicated in Figure 1C). Unexpectedly, more than 80% of the PU.1 sites localized to promoters (TSS ± 500 bp, green data points in Figure 1C) exhibited similar occupancy levels in both cell types, whereas differentially bound sites were mostly located in distal regions (Figures 1C and 1D).

To examine the relationship of PU.1 binding sites and gene expression patterns, we performed transcriptome analysis of elicited macrophages and splenic B cells and correlated binding at each PU.1 site with the mRNA level of the closest gene. Out of 17,004 genes analyzed, 58.0% and 54.9% were associated with at least one PU.1 peak in macrophages and B cells, respectively, with most of these genes exhibiting multiple peaks (Figure 1E). Genes associated with PU.1 binding were more likely to be expressed (Figure 1E), and the number of peaks per gene was positively associated with gene expression in both cell types (Figure 1F). Cell type-specific PU.1 binding was also correlated with cell type-specific gene expression (Figures 1G and S1D). Though this relationship was significant (Pearson correlation coefficient $r^2 = 0.30$, $p < 10^{-100}$), even cell type-specific genes often exhibited a mix of cell type-specific and commonly bound PU.1 peaks (e.g., Figure 1B, peak position [b]). The association between cell-specific PU.1 binding and cell-specific gene expression was strongest for peaks close to the TSS (Pearson correlation coefficient $r^2 = 0.45$, $p < 10^{-100}$); however, even the distantly located set of PU.1 peaks (>100 kb) showed correlation with vicinal gene expression ($r^2 = 0.21$, $p < 10^{-100}$). This is in line with the known distinct roles of PU.1 in both transcription initiation and enhancer function (Fisher and Scott, 1998; Lichtinger et al., 2007).

PU.1 Binds in the Vicinity of Other Lineage-Determining Transcription Factors

To gain insight into possible sequence determinants of the distinct PU.1 binding patterns observed in macrophages and B cells, we examined promoter-proximal and distal regions that were either commonly or cell type-specifically bound by PU.1 for enriched sequence elements by de novo motif analysis. The most enriched motifs were nearly identical in each of the different subsets and resembled the known PU.1 consensus element (Figures 2A and Figure S2A). The only exception was found at proximal promoter peaks common to both cell types, where PU.1 likely competes for binding with ETS factors, such as GABPα, at related ETS sites found in CpG islands (Xie et al., 2005). Though nearly 60% of all PU.1 peaks contain either the PU.1 or GABP version of ETS motifs, the most enriched motif in the remaining peaks was a degenerate ETS core motif (RRGGAASY). Overall, ~85% of all PU.1 peaks contain an ETS site, strongly suggesting that PU.1 binds directly to the vast majority of its DNA target sites (Figure 2A and Table S2).

In addition to the ETS motifs, common promoter-proximal PU.1-bound regions were highly enriched for motifs that have previously been shown to be generally enriched in promoters (Xie et al., 2005) (Figure 2A). Both promoter-proximal and promoter-distal commonly PU.1-bound regions exhibited enrichment for a PU.1:IRF composite, consistent with the ability of PU.1 and IRF4/8 to form a ternary complex on this class of composite sites in both cell types (Eisenbeis et al., 1993; Pongubala et al., 1992). In addition, promoter-distal regions bound by PU.1 in both cell types were enriched for a CTCF motif, likely because CTCF-bound sites generally coincide with accessible chromatin, as measured by DNase I hypersensitivity (Xi et al., 2007).

In striking contrast, macrophage-specific and B cell-specific PU.1-bound regions were significantly co-enriched for motifs for macrophage- and B cell-restricted, lineage-determining transcription factors, respectively (Figures 2A and 2B). This was evident to a similar degree in both promoter-proximal and promoter-distal regions (Table S2). Analysis of the spatial relationships between these co-enriched motifs and the PU.1 motif in each peak revealed that C/EBP and AP-1 motifs were highly enriched within 100 bp of macrophage-restricted distal PU.1 sites, whereas E2A, EBF, Oct, and NF-κB motifs were correspondingly highly enriched near B cell-specific distal PU.1 sites (Figures 2B, 2C, and S2B). Conversely, the B cell-specific motifs were depleted in the vicinity of macrophage-specific PU.1 sites, whereas the regions around B cell-restricted PU.1 sites were depleted of macrophage-specific motifs (Figures 2C and S2B). Secondary PU.1 motifs were also enriched within 100 bp of the central PU.1 motif, particularly at macrophage-specific and commonly bound sites (Figure S2B).

To confirm that the PU.1-co-enriched motifs were occupied by the associated cell type-restricted transcription factors, we carried out ChIP-Seq for C/EBPα and C/EBPβ in peritoneal macrophages and for Oct-2 in splenic B cells. For C/EBPα and C/EBPβ, which displayed an almost identical genomic binding pattern, we identified ~40,000 binding sites (Table S1 and Figure S2C). Of these sites, 13,840 (34.6%) were located within 100 bp of a PU.1-bound site, 60% of which were specific to macrophages, whereas only 1% were localized to B cell-specific PU.1 peaks (4 × PU.1 tag difference) (Figure 2D). For Oct-2, the number of identified sites (1191) was smaller than for the C/EBPs; however, the results complemented the above findings

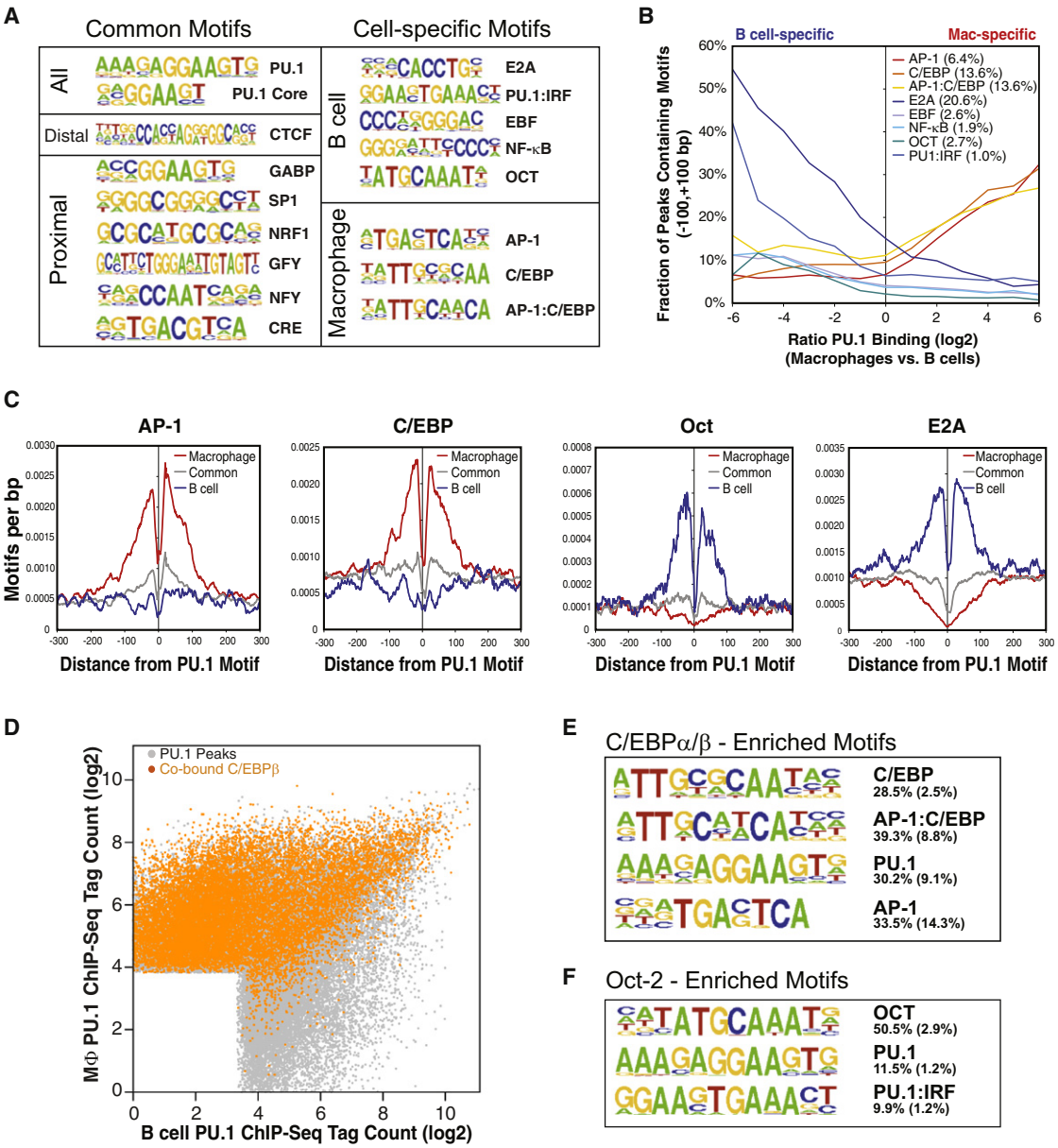

Figure 2. Transcription Factors Colocalize with PU.1 Binding Sites in Macrophages and B Cells

(A) Sequence logos corresponding to enriched sequence elements identified by de novo motif analysis of promoter-proximal or inter-/intragenic PU.1 binding sites. Motifs at PU.1 sites common to macrophages and B cells were identified by comparing common peaks to randomly selected genomic regions. Motifs enriched at PU.1 sites specific to macrophages or B cells were discovered by directly comparing the sets of peaks that were exclusive to each cell type. Motif frequencies in different subsets of PU.1 peak regions are reported in Table S2. All motifs are enriched over background with p values < 10^{-100}.

(B) Frequencies of discovered motifs in PU.1 peaks (±100 bp) as a function of differential binding of PU.1 in macrophages and B cells. Expected motif frequencies based on 100,000 random genomic regions are reported in the legend.

(C) Context-specific frequencies of AP-1, C/EBP, OCT, and E2A motifs in the vicinity of the central PU.1 motif found in PU.1 binding sites. Moving averages of motif frequencies within a 23 bp window are centered on distal macrophage-specific PU.1 sites (red), distal B cell-specific PU.1 binding sites (blue), and common distal PU.1 binding sites (gray) (>500 bp from the nearest TSS).

(D) Differential PU.1 occupancy of PU.1 peaks as in Figure 1C; PU.1 peaks are colored orange if a C/EBPβ peak is located within 100 bp of the PU.1 peak.

(E and F) Sequence logos are shown for the most highly enriched sequence motifs in C/EBPβ and Oct-2 binding sites, respectively. The fraction of peaks containing at least one instance of each motif within 100 bp of the peak center is given to the right of the motif with the expected frequency of the motif in 50,000 random regions given in parentheses.

in that 596 (50%) of all Oct-2 sites were located within 100 bp of a PU.1 peak, of which 43% were B cell specific and less than 1% macrophage specific (4 × PU.1 tag difference) (Figure S2D). C/EBP and Oct-2 binding sites exhibited similar relationships with gene expression as were observed for PU.1 (Figure S2E). C/EBP- and Oct-2-bound regions were highly enriched for C/EBP and octamer motifs, respectively (Figure 2E). In addition, C/EBP-bound regions were co-enriched for a recently described C/EBP:AP-1 composite element (Cai et al., 2008) as well as canonical PU.1 and AP-1 motifs, whereas Oct-2-bound regions in B cells were highly enriched for a PU.1 as well as a PU.1-IRF composite motif (Figure 2E).

Combinatorial Interplay Delineates Stage-Specific Cistromes

The observation that PU.1 binding occurred in the vicinity of motifs bound by lineage-restricted transcription factors prompted us to ask whether PU.1 binding to these sites was dependent on the presence of the respective factors. We addressed this question in B lineage progenitors devoid of both E2A and EBF (*E2A*$^{-/-}$), EBF only (*EBF*$^{-/-}$), or control cells that express both factors (*Rag1*$^{-/-}$), which are arrested at successive stages in B cell development (Dias et al., 2008; Ikawa et al., 2004; Lin and Grosschedl, 1995; Mombaerts et al., 1992) (Figure 1A). ChIP-Seq for PU.1 in each of these cell populations yielded 44,609, 36,908 and 17,210 peaks in *E2A*$^{-/-}$, *EBF*$^{-/-}$ and *Rag1*$^{-/-}$ progenitors, respectively (FDR < 0.1%, Table S1). Surprisingly, despite the apparent loss in total number of PU.1 peaks comparing one developmental stage to the next, each successive stage was characterized by the appearance of PU.1 sites at new genomic positions that were not occupied by PU.1 in the previous progenitor stage. Using the PU.1 sites identified in *E2A*$^{-/-}$ cells as control, de novo motif analysis of the 3760, 2479, and 9504 PU.1 sites exhibiting 3× more tags in the *EBF*$^{-/-}$, *Rag1*$^{-/-}$, and mature B cells, respectively, revealed enrichment for distinct motifs for transcription factors expressed at respective stages of B cell development (Figure 3A and Table S3), demonstrating that PU.1 binding is dependent on the activity of other lineage-determining transcription factors. For example, co-enriched E2A motifs were gained comparing the PU.1 cistrome in *EBF*$^{-/-}$ cells to that in *E2A*$^{-/-}$ cells (Figure 3A). Furthermore, gained sites were primarily associated with genomic regions corresponding to B cell-specific PU.1 binding sites in mature splenic B cells, as exemplified by the reshaping of the PU.1 binding site pattern comparing CLP/pre-pro B (*EBF*$^{-/-}$) to pro-B cells (*Rag1*$^{-/-}$) (red data points in Figure 3B).

To directly test whether the binding of PU.1 to B lineage-specific sites is dependent on E2A, we retrovirally transduced E2A-deficient CLP/pre-pro B cells derived from the bone marrow of *E2A*$^{-/-}$ mice (Ikawa et al., 2004) either with a tamoxifen-inducible E2A estrogen receptor ligand-binding domain fusion protein (E47-ER) or with the analogous construct coding for a deletion mutant of E47 that retains the bHLH DNA-binding and dimerization domain but lacks both activation domains (bHLH-ER) (Sayegh et al., 2003). Upon activation of the full-length E47-ER fusion protein with tamoxifen for 6 hr, PU.1 binding increased at 3752 sites > 4× relative to the bHLH-ER control, as exemplified by the Igκ 3′ enhancer (Figure 3C), and these sites were strongly co-enriched for an E2A motif (Figures 3D and S3A). In contrast, the PU.1 cistrome in these cells (44,609 peaks total) was not significantly altered by expression of the E2A deletion mutant lacking transcriptional activation domains (Figure 3C).

To conversely investigate whether PU.1 itself can also promote binding of one of its cistrome-associated factors, we assessed the genome-wide effects of inducing PU.1 activity on C/EBPβ binding in a PU.1-deficient (PU.1$^{-/-}$) myeloid progenitor cell line (Walsh et al., 2002). In the absence of PU.1, C/EBPβ exhibited a reduced overall binding pattern (22,641 peaks), with loss of numerous binding sites associated with locations of PU.1 binding in primary macrophages, illustrated for the macrophage-specific *Cd14* gene (PU.1KO-Cebpb versus Mac-Cebpb, Figure 3E). Motif analysis of the C/EBPβ-bound regions in *PU.1*$^{-/-}$ cells recovered C/EBP, C/EBP:AP-1, AP-1, and RUNX motifs, as well as a non-PU.1 Ets motif (AACAGGAAGT), but not the PU.1 binding motif found in primary macrophages (Figure S3G).

We next evaluated the consequences of PU.1 activity on C/EBPβ binding in *PU.1*$^{-/-}$ cells stably expressing a tamoxifen-responsive PU.1 estrogen receptor ligand-binding domain fusion protein (PUER) (Walsh et al., 2002). In this inducible system, low levels of PU.1 activity and DNA binding are observed by ChIP-Seq in the absence of tamoxifen (8144 peaks total, exemplified in Figure 3E, PUER-PU.1-0h). This low-level PU.1 activity was associated with partial recovery of C/EBPβ binding in the vicinity of some PU.1 binding sites (Figures 3E and S3H, PUER-C/EBPβ-0h). Tamoxifen treatment induced PU.1 binding to a total of 37,909 genomic regions after 1 hr and resulted in a gain of 1710 C/EBPβ binding sites (>4× tags relative to the 0 hr time point), restoring a large number of macrophage-specific PU.1 binding sites. The induced C/EBPβ binding regions were strongly enriched for a PU.1 motif (Figures 3F and S3B) and were cobound by PU.1 at more than 75% of sites. Intriguingly, 57% of PU.1 binding sites observed in the absence of tamoxifen were cobound by C/EBPβ, implying that C/EBP and related factors play an important role in directing PU.1 localization when effective PU.1 concentrations are low.

PU.1 Induces Sequential Nucleosome Remodeling and Histone H3K4 Monomethylation

Recent studies have demonstrated that lineage-determining transcription factors preferentially associate with genomic regions marked by cell type-specific patterns of histone modifications, such as monomethylation of H3K4 (H3K4me1), that are suggested to signify accessible chromatin and/or enhancer-like elements (Heintzman et al., 2009). In addition, trimethylation of H3K4 (H3K4me3) marks active and/or poised promoters (Kim et al., 2005). We therefore profiled H3K4me1 and H3K4me3 in both macrophages and B cells using ChIP-Seq and found that the majority (>80%) of PU.1-bound sites were associated with either promoter-proximal H3K4me3 or distal H3K4me1 in both cell types. Cell-specific binding of PU.1 at distal sites was highly associated with cell-specific H3K4me1 (Figure 4A). Analysis of the genomic distribution of the H3K4me1 signal averaged for all distal PU.1 binding sites revealed a bimodal pattern with a pronounced reduction of signal centered over the PU.1 binding

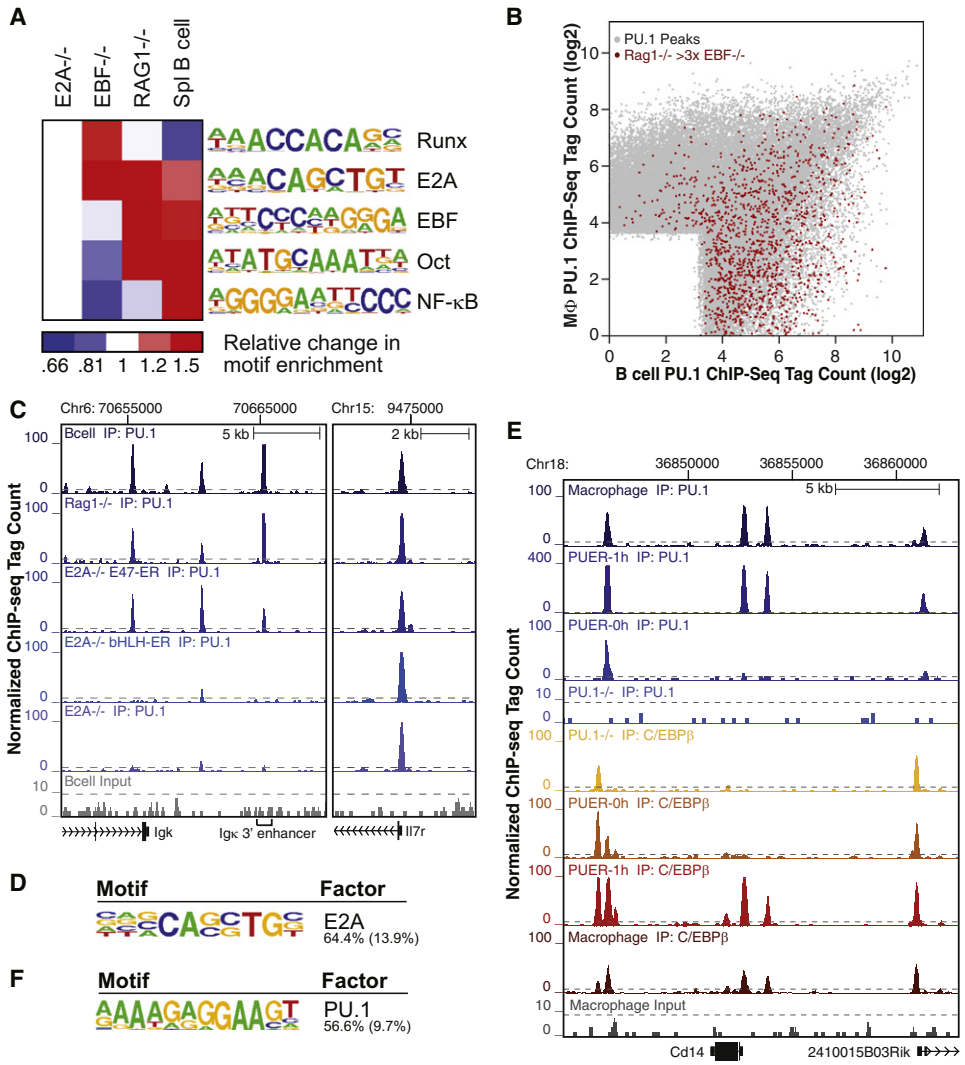

Figure 3. Cooperative Interactions between PU.1 and Cell Type-Restricted Transcription Factors Define the Macrophage and B Cell-Specific Cistromes

(A) Motifs in the vicinity of gained PU.1 sites during B cell development. Regions of 200 bp, centered on ChIP-Seq PU.1 peaks in the respective cell types, were classified according to presence or absence of a given motif. Displayed is the ratio of the fraction of gained peaks (>3-fold tag count change) containing the motif relative to the fraction of unchanged peaks (<2-fold tag count change) containing the motif. Absolute peak numbers are provided in Table S3.

(B) Same plot as in Figure 1C, with PU.1 peaks seen specifically enriched in *Rag1*$^{-/-}$ versus *EBF*$^{-/-}$ cells colored in red.

(C) UCSC browser image of the PU.1 binding pattern at the Igκ 3′ enhancer region. (Top to bottom) B cells, *Rag1*$^{-/-}$ pro-B cells, *E2A*$^{-/-}$ CLP/pre-pro-B cells reconstituted with a conditional E2A (E47-ER) or a transactivation domain-deficient E2A (bHLH-ER) 6 hr after tamoxifen treatment and *E2A*$^{-/-}$ CLP/pre-pro-B cells, as well as B cell ChIP input. The PU.1 site at the *Il7r* promoter is shown as a control for a PU.1 binding site that is invariant between the different cell types.

(D) Top motif in the vicinity of PU.1 binding sites gained following reconstitution with full-length E2A compared to constitutively bound PU.1 sites identified by de novo motif analysis. The fraction of PU.1 peaks containing at least one instance of the motif within 100 bp of the peak center in gained and constitutively bound peaks is given to the right and in parentheses, respectively.

(E) UCSC browser tracks of PU.1 and C/EBPβ binding at the CD14 locus in primary macrophages, *PU.1*$^{-/-}$ cells, and PUER cells without and 1 hr after tamoxifen treatment. (Top to bottom) PU.1 in macrophages, PUER cells after or without 1 hr tamoxifen treatment, and *PU.1*$^{-/-}$ cells (blue, dark to light) and C/EBPβ in *PU.1*$^{-/-}$ cells, PUER cells without or after 1 hr tamoxifen treatment, and macrophages (brown to red).

(F) Top motif enriched in the vicinity of gained C/EBPβ sites following activation of the PU.1-ER fusion protein compared to the constitutively bound sites identified by de novo motif analysis. The fraction of C/EBPβ peaks containing at least one instance of the motif within 100 bp of the peak center in gained and constitutively bound peaks is given to the right and in parentheses, respectively.

site (Figure 4B), analogous to that recently described for H3K4me1 around promoter-distal FoxA2- and STAT1-bound sites in mouse liver and HeLa cells, respectively (Robertson et al., 2008). Similarly, 80% of distal Oct-2 and C/EBP sites were marked by a corresponding pattern of cell-specific H3K4me1 (Figure 4B).

These observations prompted us to address the question of whether H3K4me1 serves as a beacon to recruit PU.1 and

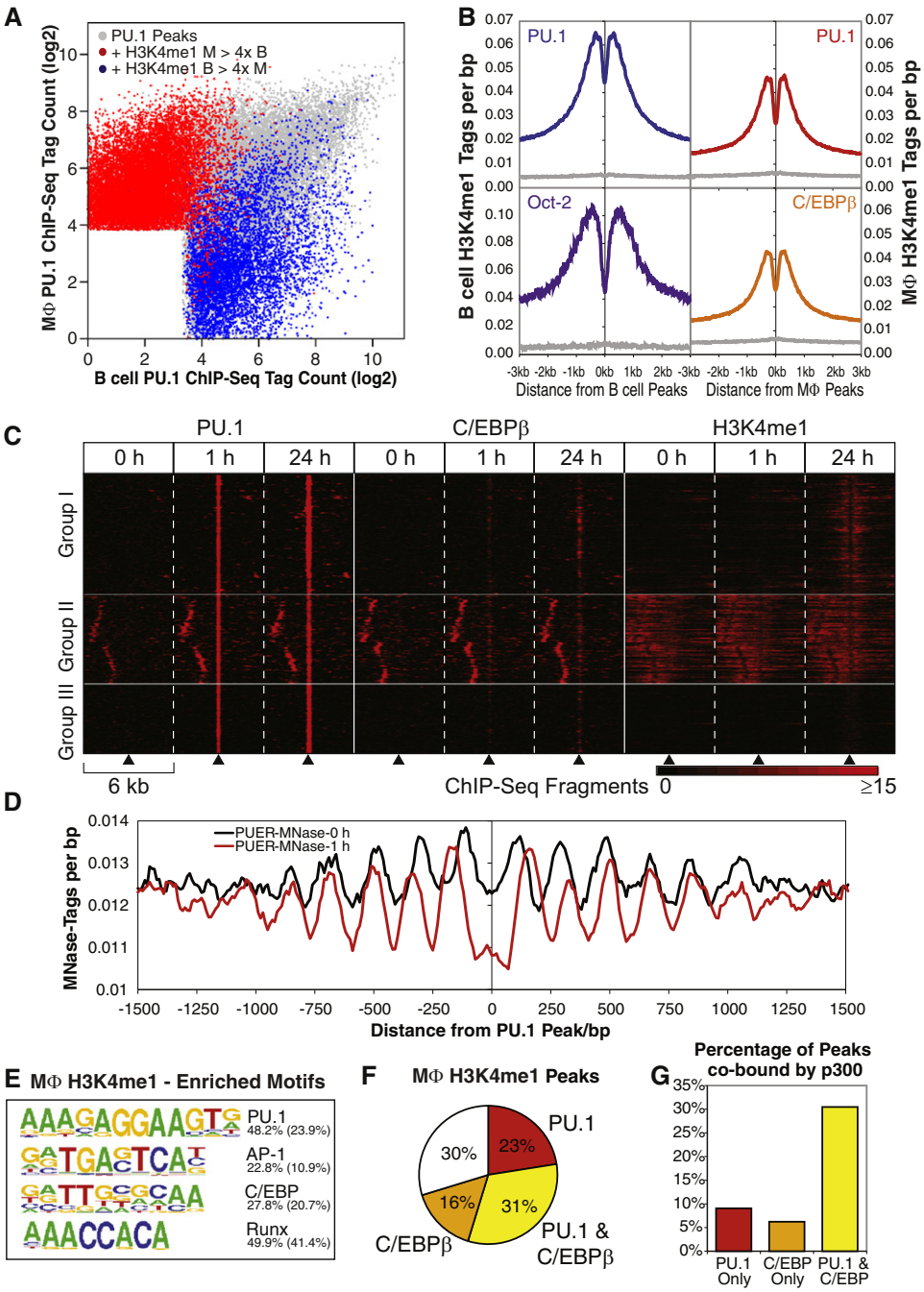

Figure 4. PU.1 and Cooperating Factors Are Required for Histone Modifications Associated with Enhancers

(A) Same plot of PU.1 peaks as in Figure 1C; peaks are colored red if the surrounding region (±500 bp) contains more than 4-fold more H3K4me1 tags in macrophages than in B cells. Peak positions fulfilling the same criteria for B cells versus macrophages are colored blue.

(B) Cell type-matched cumulative normalized H3K4me1 ChIP-Seq and input sequencing tag counts per base pair are shown around distal peak positions (>3 kb from a TSS) of PU.1 (B cells and macrophages), C/EBPβ (macrophages), and Oct-2 (B cells).

(C) Temporal and spatial relationships of PU.1, C/EBPβ, and H3K4me1 in PUER cells at different time points. Six-kb-wide regions centered on genomic sites that gained PU.1 > 6-fold after 1 hr tamoxifen were clustered according to their PU.1, C/EBPβ, and H3K4me1 ChIP-Seq profiles at 0 hr, 1 hr, or 24 hr of tamoxifen treatment. Shown are representative sections (10% of each group) of the resulting heat map.

(D) Average nucleosome positions centered on induced PU.1 peaks before and after 1 hr tamoxifen treatment as defined by MNase-Seq.

(E) Sequence motifs associated with promoter-distal H3K4me1-marked 1 kb regions in macrophages. The top four motif results from de novo motif analysis are shown. The fraction of H3K4me1-marked regions containing at least one instance of each motif within 500 bp of the peak center is given to the right of the motif, with the expected frequency of the motif in random regions in parentheses.

collaborating transcription factors and/or whether these factors are able to initiate the deposition of this mark. Using the PUER-inducible system, we performed ChIP-Seq for H3K4me1 in PUER cells at 0, 1, and 24 hr of tamoxifen treatment. Very little change in H3K4me1 signal was observed after 1 hr (38 peaks gained), but a marked increase occurred at 3328 locations by 24 hr (>4× tags, 15% of total H3K4me1 peaks present at 0 hr). To evaluate the relationship between PU.1 binding and H3K4me1, we selected a subset of 7428 highly induced PU.1 binding sites (>8-fold increase in tag count at 1 hr), which exhibited less than two tags at 0 hr. These binding sites could be classified into three groups, with representative peaks from each group shown in Figure 4C. The largest group (group I, 43%) consists of sites that gained significant H3K4me1 24 hr after PU.1 activation. This gained H3K4me1 signal exhibited a bimodal spatial distribution identical to that observed for PU.1-associated H3K4me1 in macrophages and B cells (Figure S4A). Together with the fact that 90% of the sites that gain H3K4me1 are within a 1 kb window of a gained PU.1 site, these findings suggest that PU.1 binding is required to direct the local deposition of H3K4me1 at these sites. Group II (32%) consists of induced PU.1 binding sites that were marked by pre-existing H3K4me1. In this group, PU.1 binding initiated remodeling of the local H3K4me1-containing nucleosomes at 1 hr and 24 hr, again establishing a pattern identical to that in macrophages and B cells (Figure S4A). Group III (25%) consists of peaks that, despite stable binding of PU.1, were not enriched for H3K4me1 at any time point, indicating that, here, PU.1 binding is not sufficient to establish this mark. Increased recruitment of C/EBPβ to groups I (37%) and II (30%) relative to group III (11%) peaks (<100 bp) suggests that additional factors may be required for deposition of H3K4me1. Group I and II peaks, but not group III peaks, were enriched for the 464 vicinal genes that were upregulated greater than 4-fold in PUER cells following 24 hr tamoxifen treatment (Weigelt et al., 2009) (Figure S4B).

To investigate whether the remodeling of H3K4me1-marked nucleosomes in the group II peaks was consistent with changes in nucleosomal occupancy, we mapped nucleosome positions using MNase-Seq (Schones et al., 2008) in PUER cells at 0 hr and 1 hr after treatment with tamoxifen. Analysis of the nucleosome pattern before tamoxifen treatment at the 7428 regions where PU.1 is maximally gained at 1 hr revealed a semi-regular pattern exposing the prospective PU.1 binding site on an expanded linker region between adjacent nucleosomes (Figure 4D). This pre-existing pattern is possibly due to low levels of PU.1 binding that are below detection by ChIP-Seq at the current sequencing depth, as it is possible to detect PU.1 at many of these sites in untreated PUER cells using qPCR-based ChIP assays (data not shown). Induction of PU.1 binding led to nucleosome remodeling across the entire set of induced sites, analogous to that suggested by the group II H3K4me1-marked nucleosomes, resulting in further expansion of the linker region centered on the PU.1 binding site and compression of nucleosomes in either direction along the DNA for ~1 kb. In concert, these findings suggest a sequence of events at group I sites in which PU.1 binding induces nucleosome remodeling, which is followed by monomethylation of H3K4.

Simple Combinations of Binding Sites Identify Cell Type-Specific Repertoires of H3K4me1-Marked Regions

The striking association of PU.1 and collaborating lineage-determining transcription factors with cell-specific H3K4me1 in macrophages and B cells led us to perform a de novo motif analysis of the ~20,000 distal genomic regions that were focally marked by H3K4me1 in each cell type. This analysis revealed that these regions in macrophages were most highly enriched for PU.1, AP-1, C/EBP, and RUNX motifs (Figure 4E), whereas H3K4me1-marked regions in B cells displayed maximal enrichment for PU.1, E2A, OCT, EBF, and RUNX motifs (Figure S4C). This computational result is supported by ChIP-Seq data demonstrating that the majority (70%) of the H3K4me1-positive regions in macrophages were bound by PU.1 and/or C/EBPβ (Figure 4F) and is consistent with the finding that PU.1 (and likely C/EBP) binding can induce H3K4me1 deposition. Of note, analysis of the genome-wide location of p300 in resting macrophages (Ghisletti et al., 2010) indicates marked enrichment at genomic locations cobound by PU.1 and C/EBPβ (Figure 4G).

To determine whether there is an analogous relationship between promoter-distal H3K4me1 and binding sites for transcription factors in other cell types, we performed de novo motif analysis on H3K4me1/H3K4me3 ChIP-Seq data sets from mouse embryonic stem cells (Meissner et al., 2008; Mikkelsen et al., 2007), liver (Wederell et al., 2008), human $CD4^+$ T cells (Barski et al., 2007), and $CD36^+$ erythrocyte precursors (Cui et al., 2009). Similar to the results in macrophages and B cells, H3K4me1-marked promoter-distal regions in these tissues were highly enriched for motifs for transcription factors required for the generation and maintenance of each cellular phenotype (Ivanova et al., 2006; Rothenberg and Taghon, 2005; Zaret et al., 2008) (Figure S4C). For example, H3K4me1-marked promoter-distal regions in ES cells were significantly enriched for motifs recognized by KLF4, OCT4, SOX2, and Esrrβ, factors that, in combination, are sufficient to reprogram somatic cells into induced pluripotent stem cells (Feng et al., 2009). In $CD4^+$ T cells, this analysis revealed a strong association of H3K4me1-marked regions with Ets and Runx motifs, consistent with their known essential roles in T cell development and function (Figure S4C) (Rothenberg and Taghon, 2005). In this cell type, genome-wide data for nucleosome positions, DNase hypersensitivity, and mononucleosomal ChIP-Seq for a wide range of histone modifications are available, allowing precise determination of nucleosome positions, chromatin accessibility, and histone modifications (Barski et al., 2007; Boyle et al., 2008; Schones et al., 2008). Alignment of H3K4me1 ChIP-Seq, total nucleosome sequence tag positions, and DNase I on the Ets motifs enriched in the H3K4me1-marked promoter-distal regions

(F) Pie chart depicting the overlap of PU.1 and C/EBPβ within 1 kb of focal H3K4me1 ChIP-Seq peaks.
(G) Association of p300 with PU.1 and C/EBPβ cobound sites. Percentages of transcription factor-bound regions cobound by p300 are given. Absolute numbers were: PU.1 only, 21,223 total, cobound by p300, 1,921; C/EBPβ only, 20,481 total, 1,274 with p300; PU.1 and C/EBPβ, 13,874 total, 4,230 with p300. Peak positions for p300 were determined by analysis of p300 ChIP-Seq data for resting bone marrow-derived macrophages (Ghisletti et al., 2010).

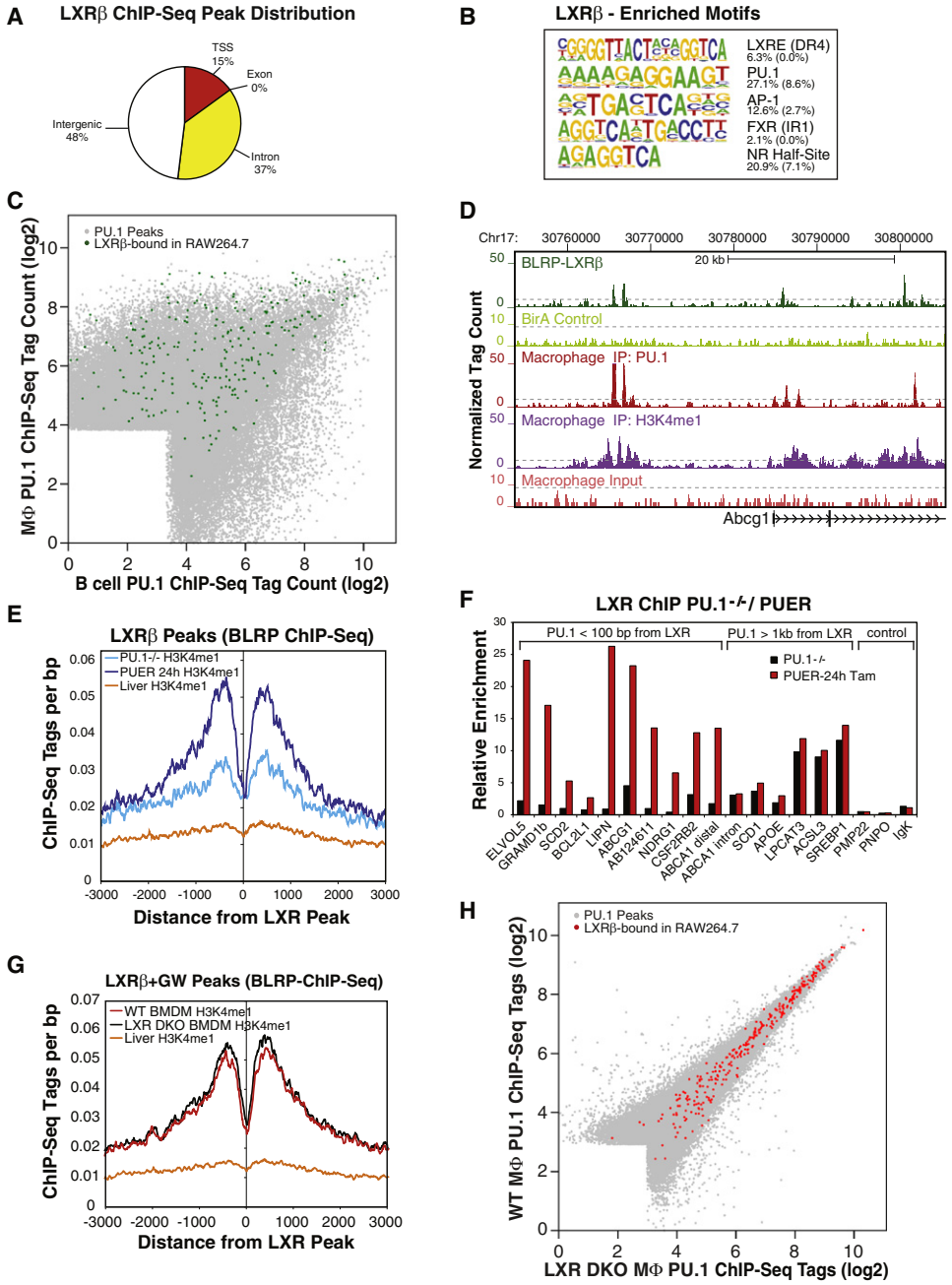

Figure 5. PU.1 Establishes Part of the LXRβ Cistrome and H3K4me1 Pattern around LXRβ Binding Sites in Macrophages, but Not Vice Versa

(A) Genomic annotation of high-confidence LXRβ binding sites defined by ChIP-Seq of biotin-tagged LXRβ in RAW264.7 murine macrophages.

(B) De novo motif analysis of LXR-bound regions in macrophages. The fraction of peaks containing at least one instance of each motif within 100 bp of the peak center is given to the right of the motif, with the expected frequency of the motif in random regions in parentheses.

(C) Macrophage and B cell PU.1 binding as in Figure 1C; PU.1 peak positions are colored green if an LXRβ peak is located within 100 bp of a PU.1 peak.

(D) UCSC browser image of the LXR target gene locus *Abcg1* depicting coordinate binding of LXR and PU.1, together with the associated H3K4me1 signature. The 2.5-fold magnified BirA control track denotes sequencing of a pull-down from formaldehyde-fixed, BirA-transgenic RAW264.7 devoid of BLRP-tagged proteins.

(E) Cumulative H3K4me1 levels in *PU.1*$^{-/-}$ myeloid progenitors (*PU.1*$^{-/-}$), PUER cells treated for 24 hr with tamoxifen (PUER 24 h), or mouse liver as control (liver H3K4me1 ChIP-Seq data from Robertson et al., 2008) around LXRβ peak positions defined in RAW264.7 macrophages.

(F) LXR binding at the indicated loci in *PU.1*$^{-/-}$ cells versus PUER cells treated with tamoxifen for 24 hr as compared by ChIP-qPCR. Values represent fold enrichment over ChIP with IgG control antibody.

(G) Cumulative H3K4me1 levels in bone marrow macrophages derived from *LXRα*$^{-/-}$/*LXRβ*$^{-/-}$ mice (LXR DKO BMDM), wild-type mice (WT BMDM), or liver (Robertson et al., 2008) as nonmacrophage control around LXRβ peak positions defined in RAW264.7 macrophages.

revealed nucleosome phasing around the Ets motif similar to the pattern that we observed around PU.1 in PUER cells, which was accompanied by a sharp spike in DNase I hypersensitivity at the Ets site (Figure S4F). This result is in stark contrast to the continuous nucleosome distribution observed when aligning the data on the means of the tag distributions (Figure S4F) and establishes that the central gap in the H3K4me1 pattern over the transcription factor motif is reflective of the absolute nucleosome positions and represents the predominant DNase I-accessible location at these promoter-distal sites.

PU.1 Establishes Cell Type-Specific Cistromes for Signal-Responsive Transcription Factors

Given the large number of transcription factors that are known to play important roles in each cell type (e.g., more than 350 transcription factors are transcribed in macrophages and ES cells; see Figure S4D), it was surprising to find that only small numbers of transcription factor motifs were highly overrepresented in the H3K4me1 patterns in the different cell types that we analyzed (Figures S4C and S4E). To explore the relationship of transcription factors whose motifs are not enriched in H3K4me1-marked regions with H3K4me1-associated factors, the global H3K4me1 pattern, and cell type-specific gene expression, we initially focused on Liver X Receptors (LXRα and LXRβ). These oxysterol-responsive nuclear receptors play numerous roles central to macrophage function by regulating target genes involved in lipid metabolism, cell survival, and immunity (Rigamonti et al., 2008).

ChIP-Seq of in vivo biotin-tagged LXRβ in the murine macrophage RAW264.7 cell line (validated in Figures S5A and S5B) identified 664 confident LXRβ binding sites (FDR < 0.1%), 85% of which were distally located relative to the TSS of vicinal genes (Figure 5A). Conventional, antibody-based ChIP assays for endogenous LXRβ in primary macrophages confirmed 12 of 12 representative LXRβ binding sites (Figure S5C). While de novo motif analysis identified the consensus LXR response element (DR4) as the most highly enriched motif, PU.1 and AP-1 motifs were also highly co-enriched in LXRβ-bound regions (Figure 5B). In line with motif enrichment, 34% of LXRβ peaks were within 100 bp of a PU.1-bound site in primary macrophages (Figure 5C), exemplified for the established LXR target gene *Abcg1* (Figure 5D). In addition, macrophage LXRβ binding sites exhibited a macrophage-specific H3K4me1 signature, in contrast to the H3K4me1 pattern around the same sites in liver (Robertson et al., 2008), another tissue in which LXRs play key regulatory roles (Figures 5E and 5G).

To determine the influence of LXRs and PU.1 on each other's DNA binding profiles, LXR binding in the absence or presence of PU.1 was compared in *PU.1*$^{-/-}$ and tamoxifen-treated PUER cells, and conversely, PU.1 binding was assessed in wild-type and in LXRα/β double-knockout bone marrow-derived macrophages. Quantitative ChIP analysis for LXRβ in *PU.1*$^{-/-}$ versus tamoxifen-treated PUER cells demonstrated that LXRβ recruitment to sites with vicinal PU.1 binding (within 100 bp) was PU.1 dependent (Figure 5F). This was not the case for LXRβ-binding sites that were not in close proximity to PU.1 (Figure 5F), indicating that PU.1 determines LXR binding in a spatially restricted manner. In concert with these findings, macrophage-specific LXRβ-bound regions displayed a significant PU.1-dependent gain in H3K4me1 signal comparing H3K4me1 ChIP-Seq profiles in *PU.1*$^{-/-}$ versus tamoxifen-treated PUER cells (Figure 5E). Conversely, the PU.1 cistrome and H3K4me1 patterns around macrophage-specific LXRβ-bound sites were not significantly altered in LXRα/β double-knockout macrophages (Figures 5G and 5H), suggesting that LXRs do not contribute to defining the PU.1 cistrome or to establishing the H3K4me1 pattern at these regions.

PU.1 Is Required for LXR and TLR-Dependent Gene Expression

Although PU.1 binding sites are significantly correlated with expression of vicinal genes (Figures 1E and 1F), an unbiased analysis of 71 sites in resting macrophages and B cells using a transient reporter gene assay revealed that a relatively small fraction (15%) conferred constitutive enhancer activity (Figure S6A). Given the finding that PU.1 participates in establishing the macrophage-specific LXR cistrome, it is possible that many of these sites might participate in defining the context- and signal-dependent transcriptional repertoire in each cell type. In support of this concept, regions containing both LXRβ and PU.1 binding sites exhibit significant sequence conservation in vertebrates, consistent with their potential importance as functional signal-responsive regulatory modules (Figure S5D). Functional analysis of representative LXR-PU.1-cobound genomic regions vicinal to LXR target genes (as defined by their responsiveness to the synthetic LXR ligand GW3965 in primary macrophages, Figure S6B) by transient reporter gene analysis in RAW264.7 cells demonstrated that 10 of 11 genomic regions that were tested exhibited ligand-dependent enhancer activity (Figure 6A). Furthermore, induction of LXR target genes in response to the LXR agonist GW3965 in PUER cells was markedly PU.1 dependent (Figure 6B).

To test whether such PU.1 dependence is a feature of other transcriptional programs defining macrophage-specific outputs, we assessed PU.1 dependence for TLR4 signaling responses in PUER cells. TLR4 ligation induces high-magnitude changes in the expression of hundreds of genes in macrophages involved in innate immune responses through the activation of numerous signal-dependent transcription factors, including NF-κB and interferon regulatory factors (Lee and Kim, 2007). Transcriptome analysis of primary macrophages treated for 6 hr with the specific TLR4 agonist Kdo2 lipid A (KLA) identified 735 genes induced more than 3-fold. PU.1 and C/EBPβ binding in resting macrophages occurred in the vicinity of 641 and 583 of these genes, respectively, and prior to KLA stimulation, these two factors colocalized, alone or together, with 537 of the 654 H3K4me1-marked regions associated with these genes (Figure 6C). Quantitative transcript analysis of 20 of these genes in the PUER system indicated that 14 required induction of PU.1

(H) Scatter plot depicting PU.1 ChIP-Seq tag counts (log2) within 200 bp of combined genomic PU.1 peak positions defined in bone marrow-derived macrophages from wild-type mice (WT MΦ) or *LXRα*$^{-/-}$/*LXRβ*$^{-/-}$ mice (LXR DKO MΦ). Genomic PU.1 peaks within 100 bp of an LXRβ peak in RAW264.7 macrophages are colored red.

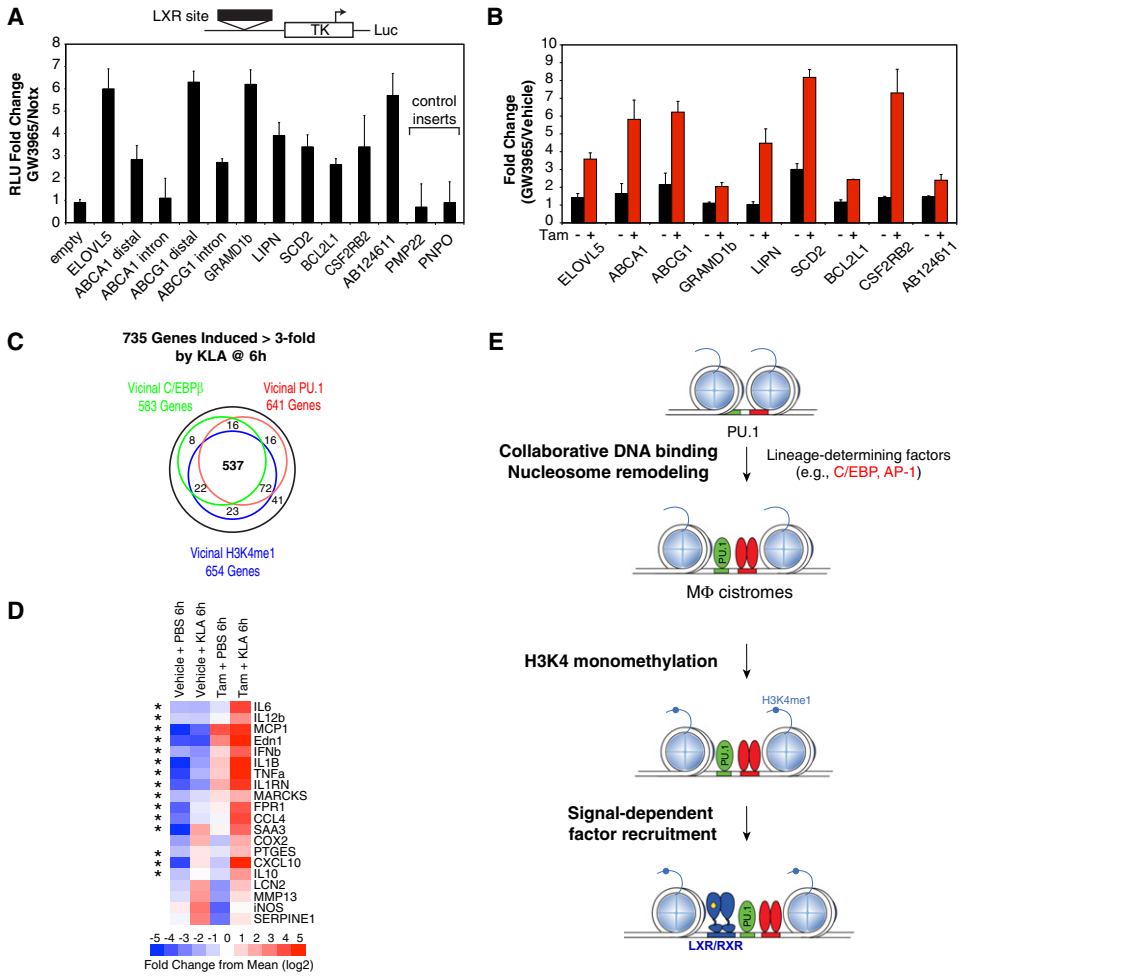

Figure 6. PU.1 Is Necessary for LXR- and TLR4-Dependent Gene Expression in Macrophages

(A) Relative enhancer activity of indicated LXR-bound regions inserted upstream of a minimal TK promoter driving luciferase expression in RAW264.7 macrophages. Data are presented as average fold change comparing 24 hr treatment with 1 μM GW3965 versus vehicle (DMSO) of three independent experiments performed in triplicate. Error bars indicate standard error of the mean (SEM).

(B) PUER cells were treated with tamoxifen or vehicle (EtOH) for 24 hr and then with 1 μM GW3965 or vehicle (DMSO) for an additional 24 hr. Average mRNA expression fold changes of the indicated genes as determined by quantitative real-time RT-PCR (qRT-PCR) comparing GW3965 versus vehicle in two independent experiments are shown. Error bars indicate standard error of the mean (SEM). All expression changes were statistically significant ($p < 0.05$, Student's t test).

(C) Overlap of vicinal PU.1, C/EBPβ, and H3K4me1 peaks in resting macrophages associated with genes that are induced more than 3-fold by KLA at 6 hr.

(D) PUER cells were treated with vehicle (DMSO) or tamoxifen for 24 hr and then with vehicle (PBS) or KLA for 6 hr. Messenger RNA levels for the indicated TLR4-responsive genes were determined by qRT-PCR and displayed as a heat map with absolute expression values ranging from low (blue) to high (red) compared to the mean level of expression for each gene. Asterisks denote genes whose KLA response is PU.1 dependent.

(E) Schematic depicting the proposed model.

binding for qualitative or substantial quantitative responses to KLA (Figure 6D). Full responses of the remainder of these genes in untreated PUER cells indicated that the TLR4-signaling pathway is functional prior to activation of PU.1.

DISCUSSION

Here, we provide evidence that collaborative interactions between PU.1 and small sets of other lineage-determining transcription factors at closely spaced binding sites establish a large proportion of their respective macrophage and B cell-specific cistromes. The spatial distributions and frequencies of the motifs for each of these factors suggest that these patterns arise from direct binding of each factor to its cognate DNA motif rather than tethering of one factor to the other. Conversely, the lack of a fixed distance between the motifs, their enrichment within 100 bp of each other, and the nucleosome remodeling observed around sites where inducible PU.1 binds in PUER cells, often in conjunction with C/EBPβ, is consistent with a mechanism in which concurrent binding of these factors enables effective competition with nucleosomes (Miller and Widom, 2003) to define cell type-specific binding patterns.

The finding that PU.1 binding leads to deposition of the H3K4me1 mark at promoter-distal sites that are correlated with cell type-specific patterns of gene expression (Heintzman et al., 2009) provides the initial evidence that PU.1 contributes to the "writing" of this epigenetic signature on a genome-wide scale. Our data also indicate that PU.1 binding and nucleosome remodeling are not sufficient to result in the deposition of this mark in all cases (Figure 4C, group III), suggesting that the mechanisms that ultimately lead to H3K4 monomethylation also require collaborative interactions with other transcription factors, such as C/EBPβ. In addition, the motifs enriched in focally H3K4me1-marked promoter-distal regions in macrophages and B cells and the shape of the H3K4me1 patterns around the binding sites of three of these factors (C/EBPα/β, Oct-2) suggest that the other H3K4me1-associated factors are also involved in nucleosome displacement and targeting of H3K4me1 deposition around their binding sites. The observation that H3K4me1-marked regions in other tissues and cell types, including liver, erythrocytes, T cells, and ES cells, also exhibit enrichment for limited sets of motifs for corresponding lineage determining factors (Figure S4C) suggests a general approach to the identification of such factors in distinct cell types, knowledge of which may facilitate cellular reprogramming efforts.

Taken together, our findings support a model in which two tiers of transcription factors cooperate to activate *cis*-active regulatory elements required for the development and function of macrophages and B cells (Figure 6E). The first tier consists of relatively small sets of lineage-determining factors, such as PU.1, C/EBPs, and E2A, that act in a collaborative manner to delineate large sets of potential *cis*-regulatory elements in a cell type-specific fashion (exemplified for macrophages in Figure 6E). The specific attributes of these factors that enable this role remain to be defined but presumably include expression levels and the ability to engage nucleosome-remodeling factors and ultimately histone-modifying enzymes that generate an accessible "proto-enhancer" structure. Consistent with this, wild-type E2A induces PU.1 binding at B cell-specific genomic sites that contain closely spaced PU.1 and E2A motifs, whereas a mutant form of E2A that is competent to bind to DNA but lacks transcriptional activation function does not (Figure 3C). This result highlights an important role for transactivation domains in enabling combinatorial transcription factor binding to chromatinized DNA at enhancer-like elements, in addition to their known roles in transcription initiation.

We provide further evidence that the priming of *cis*-active elements by lineage-determining factors is required for the subsequent binding of a second tier of factors, exemplified by LXRs (Figure 6E) and transcription factors that are activated by TLR4 signaling. This interpretation is supported by the recent observation that recruitment of p300 to new genomic locations in macrophages in response to TLR4 activation primarily occurs at regions exhibiting pre-existing H3K4me1 (Ghisletti et al., 2010), which, from our analysis, largely are sites of combinatorial interactions of PU.1, C/EBP, and AP-1 transcription factors. Collectively, these sequential events lead to a functionally active enhancer capable of contributing to cell type-specific and/or signal-dependent gene expression, similar to the sequential steps leading to activation of the *Csf1r* locus during macrophage development (Krysinska et al., 2007). This model offers an explanation for the extensive genome-wide and cell type-specific colocalization of transcription factors observed in various previous studies (Chen et al., 2008; MacArthur et al., 2009) and provides insights into how simple combinations of lineage-restricted transcription factors on a genome-wide scale can specify promoter-distal *cis*-regulatory elements ultimately responsible for both cell identity and cell type-specific responses to diverse signaling inputs.

EXPERIMENTAL PROCEDURES

Cell Isolation and Culture

Primary cells were isolated from male 6- to 8-week-old C57Bl/6 mice (Charles River Laboratories). Peritoneal macrophages were harvested by peritoneal lavage 3 days after i.p. injection of 3 ml thioglycollate, overnight culture, and adherence selection. BMDM were generated as described (Valledor et al., 2004). Splenic B cells were isolated by magnetic depletion of CD43- and CD11b-expressing cells (Miltenyi). $B220^+$ pro-B cells were magnetically enriched from bone marrow of Rag1 knockout mice and expanded for 10 days as described (Sayegh et al., 2005) with slight modifications. $E2A^{-/-}$ and $EBF^{-/-}$ pre-pro-B cells were cultured as described previously (Ikawa et al., 2004). $PU.1^{-/-}$ and PUER cells were propagated, and the PU.1-ER fusion protein was activated with 100 nM 4-hydroxy-tamoxifen as described (Walsh et al., 2002).

Microarray Analysis

Gene expression profiling was performed in biological duplicates on 44K Whole Mouse Genome Oligo Microarrays (Agilent) according to the manufacturer's instructions.

Retroviral Transduction

E47-ER-Tac and bHLH-ER-Tac retroviral constructs were described (Sayegh et al., 2003). Virus was generated by transfection of the constructs and packaging vector into HEK293T cells. E2A-deficient hematopoietic progenitor cells were transduced as described previously (Quong et al., 1999). After 18 hr, E47-ER and bHLH-ER were activated for 6 hr with 1 μM 4-hydroxy-tamoxifen, and transduced cells were magnetically enriched (Miltenyi) for bicistronically coexpressed human CD25 (TAC antigen).

Chromatin Immunoprecipitation

Chromatin immunoprecipitation (ChIP) was performed with 10–20 × 10^6 cells essentially as described (Métivier et al., 2003). Antibodies used: PU.1 (sc-352), C/EBPα (sc-61), C/EBPβ (sc-150), Oct-2 (sc-233) and pan-LXR (sc-1000) (Santa Cruz Biotech), H3K4me1 (ab8895) and H3K4me3 (ab8580) (Abcam), or LXRβ (PP-K8917-00, Perseus Proteomics).

MNase-Seq

Micrococcal nuclease digest and deep sequencing (MNase-Seq) was essentially performed as described (Schones et al., 2008).

High-Throughput Sequencing

Library preparation and high-throughput sequencing for 36 cycles was performed on Illumina Genome Analyzers I and II according to the manufacturer's protocols (Illumina). The first 23–25 bp of each sequence tag were mapped to the mm8 assembly (NCBI build 36). Tag counts for each experiment were normalized to 10^7 specifically mapped tags.

Data Analysis

Peak finding and downstream data analysis was performed using HOMER, a software suite for ChIP-Seq analysis, which in part was created to support this study. Peaks were defined at a 0.1% estimated false discovery rate, indicated as a dashed line in genome browser images.

ACCESSION NUMBERS

Sequencing and gene expression data are available in the Gene Expression Omnibus database (http://www.ncbi.nlm.nih.gov/geo) under the accession number GSE21512.

SUPPLEMENTAL INFORMATION

Supplemental Information includes Supplemental Experimental Procedures, six figures, and three tables and can be found with this article online at doi:10.1016/j.molcel.2010.05.004.

ACKNOWLEDGMENTS

We thank Dr. Bing Ren, Dr. Michael Rehli, and Dr. Constanze Bonifer for discussions and reading of the manuscript; Dr. Gary Hardiman and especially Colleen Ludka for assistance with Solexa sequencing; Rosa Luna for technical assistance; Dr. Young-Soo Kwon for suggestions and discussions; and Lynn Bautista for assistance with manuscript preparation. S.H. was supported by an NIH postdoctoral training grant (F32 HL083752). These studies were primarily funded by NURSA consortium grant number DK62434 and further supported by NIH grants to C.K.G. (HC088093, DK063491, CA52599), H.S. (P50 GM081892), and C.M. (R01 CA078384), and a Foundation Leducq Transatlantic Network Grant to C.K.G. H.S. acknowledges HHMI support.

Received: February 3, 2010
Revised: April 2, 2010
Accepted: May 3, 2010
Published: May 27, 2010

REFERENCES

Adolfsson, J., Månsson, R., Buza-Vidas, N., Hultquist, A., Liuba, K., Jensen, C.T., Bryder, D., Yang, L., Borge, O.J., Thoren, L.A., et al. (2005). Identification of Flt3+ lympho-myeloid stem cells lacking erythro-megakaryocytic potential a revised road map for adult blood lineage commitment. Cell *121*, 295–306.

Barski, A., Cuddapah, S., Cui, K., Roh, T.Y., Schones, D.E., Wang, Z., Wei, G., Chepelev, I., and Zhao, K. (2007). High-resolution profiling of histone methylations in the human genome. Cell *129*, 823–837.

Boyes, J., and Felsenfeld, G. (1996). Tissue-specific factors additively increase the probability of the all-or-none formation of a hypersensitive site. EMBO J. *15*, 2496–2507.

Boyle, A.P., Davis, S., Shulha, H.P., Meltzer, P., Margulies, E.H., Weng, Z., Furey, T.S., and Crawford, G.E. (2008). High-resolution mapping and characterization of open chromatin across the genome. Cell *132*, 311–322.

Cai, D.H., Wang, D., Keefer, J., Yeamans, C., Hensley, K., and Friedman, A.D. (2008). C/EBP alpha:AP-1 leucine zipper heterodimers bind novel DNA elements, activate the PU.1 promoter and direct monocyte lineage commitment more potently than C/EBP alpha homodimers or AP-1. Oncogene *27*, 2772–2779.

Chen, X., Xu, H., Yuan, P., Fang, F., Huss, M., Vega, V.B., Wong, E., Orlov, Y.L., Zhang, W., Jiang, J., et al. (2008). Integration of external signaling pathways with the core transcriptional network in embryonic stem cells. Cell *133*, 1106–1117.

Cirillo, L.A., Lin, F.R., Cuesta, I., Friedman, D., Jarnik, M., and Zaret, K.S. (2002). Opening of compacted chromatin by early developmental transcription factors HNF3 (FoxA) and GATA-4. Mol. Cell *9*, 279–289.

Cui, K., Zang, C., Roh, T.Y., Schones, D.E., Childs, R.W., Peng, W., and Zhao, K. (2009). Chromatin signatures in multipotent human hematopoietic stem cells indicate the fate of bivalent genes during differentiation. Cell Stem Cell *4*, 80–93.

Dias, S., Månsson, R., Gurbuxani, S., Sigvardsson, M., and Kee, B.L. (2008). E2A proteins promote development of lymphoid-primed multipotent progenitors. Immunity *29*, 217–227.

Eisenbeis, C.F., Singh, H., and Storb, U. (1993). PU.1 is a component of a multiprotein complex which binds an essential site in the murine immunoglobulin lambda 2-4 enhancer. Mol. Cell. Biol. *13*, 6452–6461.

Feng, B., Jiang, J., Kraus, P., Ng, J.H., Heng, J.C., Chan, Y.S., Yaw, L.P., Zhang, W., Loh, Y.H., Han, J., et al. (2009). Reprogramming of fibroblasts into induced pluripotent stem cells with orphan nuclear receptor Esrrb. Nat. Cell Biol. *11*, 197–203.

Fisher, R.C., and Scott, E.W. (1998). Role of PU.1 in hematopoiesis. Stem Cells *16*, 25–37.

Friedman, A.D. (2007). Transcriptional control of granulocyte and monocyte development. Oncogene *26*, 6816–6828.

Ghisletti, S., Barozzi, I., Mietton, F., Polletti, S., De Santa, F., Venturini, E., Gregory, L., Lonie, L., Chew, A., Wei, C.L., et al. (2010). Identification and characterization of enhancers controlling the inflammatory gene expression program in macrophages. Immunity *32*, 317–328.

Heintzman, N.D., Hon, G.C., Hawkins, R.D., Kheradpour, P., Stark, A., Harp, L.F., Ye, Z., Lee, L.K., Stuart, R.K., Ching, C.W., et al. (2009). Histone modifications at human enhancers reflect global cell-type-specific gene expression. Nature *459*, 108–112.

Ikawa, T., Kawamoto, H., Wright, L.Y., and Murre, C. (2004). Long-term cultured E2A-deficient hematopoietic progenitor cells are pluripotent. Immunity *20*, 349–360.

Ivanova, N., Dobrin, R., Lu, R., Kotenko, I., Levorse, J., DeCoste, C., Schafer, X., Lun, Y., and Lemischka, I.R. (2006). Dissecting self-renewal in stem cells with RNA interference. Nature *442*, 533–538.

Kim, T.H., Barrera, L.O., Zheng, M., Qu, C., Singer, M.A., Richmond, T.A., Wu, Y., Green, R.D., and Ren, B. (2005). A high-resolution map of active promoters in the human genome. Nature *436*, 876–880.

Krysinska, H., Hoogenkamp, M., Ingram, R., Wilson, N., Tagoh, H., Laslo, P., Singh, H., and Bonifer, C. (2007). A two-step, PU.1-dependent mechanism for developmentally regulated chromatin remodeling and transcription of the c-fms gene. Mol. Cell. Biol. *27*, 878–887.

Lee, M.S., and Kim, Y.J. (2007). Signaling pathways downstream of pattern-recognition receptors and their cross talk. Annu. Rev. Biochem. *76*, 447–480.

Lichtinger, M., Ingram, R., Hornef, M., Bonifer, C., and Rehli, M. (2007). Transcription factor PU.1 controls transcription start site positioning and alternative TLR4 promoter usage. J. Biol. Chem. *282*, 26874–26883.

Lin, H., and Grosschedl, R. (1995). Failure of B-cell differentiation in mice lacking the transcription factor EBF. Nature *376*, 263–267.

Lupien, M., Eeckhoute, J., Meyer, C.A., Wang, Q., Zhang, Y., Li, W., Carroll, J.S., Liu, X.S., and Brown, M. (2008). FoxA1 translates epigenetic signatures into enhancer-driven lineage-specific transcription. Cell *132*, 958–970.

MacArthur, S., Li, X.Y., Li, J., Brown, J.B., Chu, H.C., Zeng, L., Grondona, B.P., Hechmer, A., Simirenko, L., Keränen, S.V., et al. (2009). Developmental roles of 21 Drosophila transcription factors are determined by quantitative differences in binding to an overlapping set of thousands of genomic regions. Genome Biol. *10*, R80.

Medina, K.L., and Singh, H. (2005). Gene regulatory networks orchestrating B cell fate specification, commitment, and differentiation. Curr. Top. Microbiol. Immunol. *290*, 1–14.

Meissner, A., Mikkelsen, T.S., Gu, H., Wernig, M., Hanna, J., Sivachenko, A., Zhang, X., Bernstein, B.E., Nusbaum, C., Jaffe, D.B., et al. (2008). Genome-scale DNA methylation maps of pluripotent and differentiated cells. Nature *454*, 766–770.

Métivier, R., Penot, G., Hübner, M.R., Reid, G., Brand, H., Kos, M., and Gannon, F. (2003). Estrogen receptor-alpha directs ordered, cyclical, and combinatorial recruitment of cofactors on a natural target promoter. Cell *115*, 751–763.

Mikkelsen, T.S., Ku, M., Jaffe, D.B., Issac, B., Lieberman, E., Giannoukos, G., Alvarez, P., Brockman, W., Kim, T.K., Koche, R.P., et al. (2007). Genome-wide maps of chromatin state in pluripotent and lineage-committed cells. Nature *448*, 553–560.

Miller, J.A., and Widom, J. (2003). Collaborative competition mechanism for gene activation in vivo. Mol. Cell. Biol. *23*, 1623–1632.

Mombaerts, P., Iacomini, J., Johnson, R.S., Herrup, K., Tonegawa, S., and Papaioannou, V.E. (1992). RAG-1-deficient mice have no mature B and T lymphocytes. Cell *68*, 869–877.

Odom, D.T., Zizlsperger, N., Gordon, D.B., Bell, G.W., Rinaldi, N.J., Murray, H.L., Volkert, T.L., Schreiber, J., Rolfe, P.A., Gifford, D.K., et al. (2004). Control of pancreas and liver gene expression by HNF transcription factors. Science *303*, 1378–1381.

Pongubala, J.M., Nagulapalli, S., Klemsz, M.J., McKercher, S.R., Maki, R.A., and Atchison, M.L. (1992). PU.1 recruits a second nuclear factor to a site important for immunoglobulin kappa 3′ enhancer activity. Mol. Cell. Biol. *12*, 368–378.

Quong, M.W., Harris, D.P., Swain, S.L., and Murre, C. (1999). E2A activity is induced during B-cell activation to promote immunoglobulin class switch recombination. EMBO J. *18*, 6307–6318.

Rigamonti, E., Chinetti-Gbaguidi, G., and Staels, B. (2008). Regulation of macrophage functions by PPAR-alpha, PPAR-gamma, and LXRs in mice and men. Arterioscler. Thromb. Vasc. Biol. *28*, 1050–1059.

Robertson, A.G., Bilenky, M., Tam, A., Zhao, Y., Zeng, T., Thiessen, N., Cezard, T., Fejes, A.P., Wederell, E.D., Cullum, R., et al. (2008). Genome-wide relationship between histone H3 lysine 4 mono- and tri-methylation and transcription factor binding. Genome Res. *18*, 1906–1917.

Rothenberg, E.V., and Taghon, T. (2005). Molecular genetics of T cell development. Annu. Rev. Immunol. *23*, 601–649.

Sandmann, T., Jensen, L.J., Jakobsen, J.S., Karzynski, M.M., Eichenlaub, M.P., Bork, P., and Furlong, E.E. (2006). A temporal map of transcription factor activity: mef2 directly regulates target genes at all stages of muscle development. Dev. Cell *10*, 797–807.

Sayegh, C.E., Quong, M.W., Agata, Y., and Murre, C. (2003). E-proteins directly regulate expression of activation-induced deaminase in mature B cells. Nat. Immunol. *4*, 586–593.

Sayegh, C.E., Sayegh, C., Jhunjhunwala, S., Riblet, R., and Murre, C. (2005). Visualization of looping involving the immunoglobulin heavy-chain locus in developing B cells. Genes Dev. *19*, 322–327.

Schones, D.E., Cui, K., Cuddapah, S., Roh, T.Y., Barski, A., Wang, Z., Wei, G., and Zhao, K. (2008). Dynamic regulation of nucleosome positioning in the human genome. Cell *132*, 887–898.

Tronche, F., and Yaniv, M. (1992). HNF1, a homeoprotein member of the hepatic transcription regulatory network. Bioessays *14*, 579–587.

Valledor, A.F., Hsu, L.C., Ogawa, S., Sawka-Verhelle, D., Karin, M., and Glass, C.K. (2004). Activation of liver X receptors and retinoid X receptors prevents bacterial-induced macrophage apoptosis. Proc. Natl. Acad. Sci. USA *101*, 17813–17818.

Verger, A., and Duterque-Coquillaud, M. (2002). When Ets transcription factors meet their partners. Bioessays *24*, 362–370.

Walsh, J.C., DeKoter, R.P., Lee, H.J., Smith, E.D., Lancki, D.W., Gurish, M.F., Friend, D.S., Stevens, R.L., Anastasi, J., and Singh, H. (2002). Cooperative and antagonistic interplay between PU.1 and GATA-2 in the specification of myeloid cell fates. Immunity *17*, 665–676.

Wederell, E.D., Bilenky, M., Cullum, R., Thiessen, N., Dagpinar, M., Delaney, A., Varhol, R., Zhao, Y., Zeng, T., Bernier, B., et al. (2008). Global analysis of in vivo Foxa2-binding sites in mouse adult liver using massively parallel sequencing. Nucleic Acids Res. *36*, 4549–4564.

Weigelt, K., Lichtinger, M., Rehli, M., and Langmann, T. (2009). Transcriptomic profiling identifies a PU.1 regulatory network in macrophages. Biochem. Biophys. Res. Commun. *380*, 308–312.

Xi, H., Shulha, H.P., Lin, J.M., Vales, T.R., Fu, Y., Bodine, D.M., McKay, R.D., Chenoweth, J.G., Tesar, P.J., Furey, T.S., et al. (2007). Identification and characterization of cell type-specific and ubiquitous chromatin regulatory structures in the human genome. PLoS Genet. *3*, e136.

Xie, X., Lu, J., Kulbokas, E.J., Golub, T.R., Mootha, V., Lindblad-Toh, K., Lander, E.S., and Kellis, M. (2005). Systematic discovery of regulatory motifs in human promoters and 3′ UTRs by comparison of several mammals. Nature *434*, 338–345.

Zaret, K.S., Watts, J., Xu, J., Wandzioch, E., Smale, S.T., and Sekiya, T. (2008). Pioneer factors, genetic competence, and inductive signaling: programming liver and pancreas progenitors from the endoderm. Cold Spring Harb. Symp. Quant. Biol. *73*, 119–126.